

Evaluation of the Virtual Crystal Approximation for Predicting Alloy Phonon Properties and Thermal Conductivity

Jason M. Larkin¹ and A. J. H. McGaughey^{1,*}

¹*Department of Mechanical Engineering*

Carnegie Mellon University

Pittsburgh, PA 15213

(Dated: February 16, 2013)

The virtual crystal approximation for mass disorder is evaluated by examining two model alloy systems: Lennard-Jones argon and Stillinger-Weber silicon. In both cases the perfect crystal is alloyed with a heavier mass species up to equal concentration and phonon frequencies, lifetimes and group velocities and thermal conductivity are predicted. These two alloy systems have different ranges of phonon frequencies, lifetimes. For Stillinger-Weber silicon, the virtual crystal approximation predicts phonon properties and thermal conductivity in reasonably good agreement with molecular dynamics-based methods. For Lennard-Jones argon, the virtual crystal approximation underpredicts the high-frequency phonon lifetimes, leading to an underpredicting of its thermal conductivity. Resolution of this underprediction is achieved by considering methods that treat the disorder explicitly.

I. INTRODUCTION

Disordered materials (i.e., alloys and amorphous solids) are used in applications ranging from semiconducting devices to thermally insulating barriers due to their low thermal conductivities.(cite) For example, reducing the thermal conductivity of thermoelectric materials can improve the efficiency of thermoelectric devices.(cite) Theoretical predictions of thermal conductivity of disordered lattices dates back to the work of Abeles, who showed that mass and strain disorder dominate the thermal resistivity of Si-Ge and (Ga,In)-As alloys, respectively.¹

Alloying, introducing mass or bond disorder to ordered lattices, remains an effective method to reduce the thermal conductivity while maintaining good electrical transport properties.(cite) In particular, for materials with short phonon mean free paths, alloying is a potential thermal conductivity reduction mechanism where nanosstructuring is not.^{2,3} In the case of dielectrics, almost all of the heat is conducted by the vibrational modes of the system. Understanding how these vibrations contribute to thermal transport is crucial for predicting the thermal conductivity of ordered and disordered lattices.

Accurately predicting the thermal conductivity of a dielectric or semiconducting material requires the properties of the vibrations from the entire Brillouin zone.^{4,5} Accurate predictions of these properties for bulk systems can be made with anharmonic lattice dynamics (ALD) theory using *ab initio* calculations.^{3,6–11} However, computational costs limit the size of computational cells in *ab initio* calculations to be less than 100 atoms, making it difficult to explicitly incorporate the effects of disorder.^{3,7,8,12,13}

Recently, work using *ab initio* calculations, anharmonic lattice dynamics (ALD), and the virtual crystal (VC) approximation predicted phonon mode frequencies,

lifetimes and group velocities of defected materials with relatively large (order 100 W/m-K^{7,8}) and small (order 1 W/m-K³) thermal conductivities. Under the VC approximation, the disordered solid is replaced with a perfect virtual crystal with properties equivalent to an averaging over the disorder (e.g., mass or bond strength).¹ The use of ALD with the VC approximation (referred to herein as VC-ALD) can base all calculations on a small unit cell with averaged properties and treat the effects of intrinsic and disorder scattering as perturbations.^{1,3,7,14} No comprehensive study has been performed to assess the applicability of this perturbative approach for a range of disorder (varying alloy concentrations, Section) using multiple predictive methods and test systems.

The goal of this work is to investigate the use of the VC approximation for predicting vibrational mode properties and thermal conductivity of alloys by a detailed comparison of three predictive methods: (i) Molecular Dynamics (MD)-based normal mode decomposition (NMD, Section) and green-kubo (GK, Section ??), and VC-ALD (Section III C 2). Using the VC approximation, we perform calculations at different concentrations (c) of mass varying binary alloys of Lennard-Jones argon and Stillinger-Weber silicon (Section). We predict the phonon mode properties of the VC: frequencies (Section), group velocities (Section), and lifetimes (Section), and use them to predict thermal conductivity (Section). In both cases, the perfect lattice is disordered with a heavier mass species up to equal concentration ($c = 0.5$), spanning a range of perturbative to large disorder. By spanning this range, the limits of the perturbative models are examined.

Using computationally-cheap empirical potentials for argon(cite) and silicon¹⁵, we study the effects of disorder explicitly. Methods referred to as VC-NMD (Section) and VC-ALD (Section) use the VC approximation. Explicit disorder is examined using lattice dynamics (LD)

calculations (Section and), MD simulations (Section), and Allen-Feldman (AF) theory (Section).¹⁶ The breakdown of the perturbative VC-ALD method is examined (Section), and a simple correction is suggested by predictions from the AF theory (Section).

II. THEORETICAL AND MODELING FORMULATION

A. Thermal Conductivity Predictions

To predict the thermal conductivity of disordered lattices, one begins with the theory for a perfect lattice. For a perfect lattice, all vibrational modes are phonon modes, which by definition are delocalized, propagating plane waves.(cite) Using the single-mode relaxation time approximation⁴ to solve the Boltzmann transport equation¹⁷ gives an expression for thermal conductivity,

$$k_{ph,\mathbf{n}} = \sum_{\boldsymbol{\kappa}} \sum_{\nu} c_{ph}(\boldsymbol{\kappa}_{\nu}) v_{g,\mathbf{n}}^2(\boldsymbol{\kappa}_{\nu}) \tau(\boldsymbol{\kappa}_{\nu}). \quad (1)$$

Here, the phonon mode has frequency $\omega(\boldsymbol{\kappa}_{\nu})$, c_{ph} is the phonon volumetric specific heat, $v_{g,\mathbf{n}}$ is the component of the group velocity vector in direction \mathbf{n} , and $\tau(\boldsymbol{\kappa}_{\nu})$ is the phonon lifetime.

The SMRT approximation has been shown to be accurate for SiGe alloys and lower thermal conductivity materials, while larger conductivity materials such as GaN and Diamond require a full iterative solution to the BTE for more accurate predictions.^{6–8} For the perfect cubic lattices considered in this work (see Section), the lattices and the components of their thermal conductivity are cubically symmetric, so that we refer to k_{ph} as a scalar thermal conductivity. This is also true for the disordered lattices in the infinite size limit. Since MD simulations are classical and obey Maxwell-Boltzmann statistics,¹⁸ the volumetric specific heat is k_B/V per mode in the harmonic limit, where V is the system volume. This approximation has been shown to be valid for LJ Ar(cite SED) and SW Si(cite SED) and is used in this work so that direct comparisons can be made between methods.

For disordered systems, the vibrational modes of the system are no longer pure plane-waves (phonon modes), except in the low-frequency (long-wavelength) limit. The Allen-Feldman (AF) theory computes the contribution of diffusive, non-propagating modes to vibrational conductivity.¹⁶ In the AF theory, the thermal conductivity is written as

$$k_{AF} = \sum_{modes} \frac{k_B}{V} D_{AF}(\omega), \quad (2)$$

where D_{AF} is the mode-specific thermal diffusivity of disordered vibrational modes defined at the wavevector [000]. The relative contribution of both phonons and diffusons to the total vibrational conductivity, $k_{vib} = k_{ph} + k_{AF}$, has been estimated to be approximately equal

for a-Si,¹⁹ while earlier studies find that k_{ph} is substantially less.²⁰ While studies have been performed on alloying the amorphous phase, the AF theory has not been applied to disordered lattices.⁵ In the current study of disordered lattices, the AF theory predictions provide a lower limit for the contribution of a given vibrational mode within the computational framework of the VC approximation (Section). This is essential given the computational cost of the AF theory (Appendix), and is also convenient given the simplicity of the VC computational framework.

B. Virtual Crystal Approximation

Abeles first introduced the idea of using a virtual crystal (VC) to replace a disordered one, computing the thermal conductivity of SiGe, (Ga,In)As and In(As,P) in good agreement with experimental results. The Abeles theory is conceptually simple, treating both disorder and anharmonicity as perturbations.¹ Deviations from the Abeles theory were observed for In(As,P) at large concentrations, which was attributed to the high mass ratio of 3.7 for InP.¹

While the Abeles theory is valid for perturbative disorder, its use leads to good agreement with several experimental and computational results for systems with a range of disorder. Cahill and co-workers found that conductivity reduction in dilute Ge-doped Si epitaxial layers can be explained by mass perturbative disorder.^{21,22} While the mass ratio was large ($m_{Ge}/m_{Si} = 2.6$), the overall disorder strength is determined by both the mass ratio and the alloy concentration (Section). As little as $6.2 \times 10^{19} cm^{-3}$ Ge is enough to reduce the thermal conductivity of Si by almost a factor of 2.²¹ In the case of $Ni_{0.55}Pd_{0.45}$, with large mass disorder and concentration ($m_{Pd}/m_{Ni} \approx 2$), good agreement is seen using the VC approach.²³ Given these experimental results, it is unclear what limitations exist using the VC approach for arbitrary disorder.

Computational results using the VC approximation for high thermal conductivity alloys show good to excellent agreement with experimental results for small and large concentrations.^{7,8} Lindsay and Broido found good agreement with VC-ALD and experiment for isotopically defected GaN with relatively small concentrations.⁷ Garg used ab initio calculations with VC-ALD to predict the thermal conductivity of SiGe alloys for all concentrations, obtaining excellent agreement with experiment.⁸ Isotopically defected GaN and SiGe alloys have relatively large thermal conductivities.(cite) In particular, the conductivity of SiGe alloys is significantly larger than that of the high scatter limit.²⁴ For both experiment and numerical modeling, VC predictions tend to be accurate when the thermal conductivity is significantly above the high-scatter limit.^{1,7,8,21–24}

A detailed study of low thermal conductivity materials PbTe⁹ and PbTe/PbSe³ made predictions for the per-

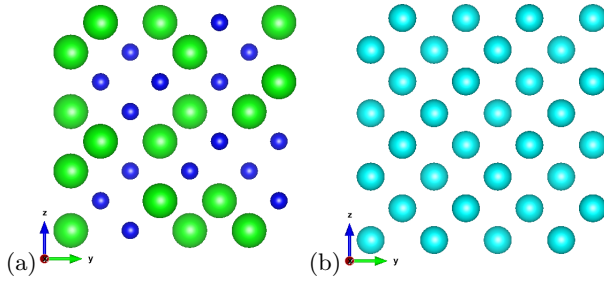


FIG. 1: (a) view of an explicitly disordered supercell of Si and “heavy” Si ([100] direction into the paper).⁷ (b) view of the equivalent VC supercell with an average mass of the explicitly disordered Si and “heavy” Si supercell (b). Sphere size represents increasing mass only, no bond disorder is considered. In this work, calculations for LJ Ar and SW Si which use the VC approximation are based off of the conventional cubic unit cells (Section III A, ??, III C 1 and III C 2). The explicitly disordered supercells are used in Sections III A, III B 2, III C 1 and ??.

fect systems in fair agreement with experiment, where results lack for the alloys. The thermal conductivity of PbTe/PbSe and their alloys have thermal conductivities at thermoelectric operating temperatures which approach the high scatter limit.(cite) Thus, there is a need to examine the perturbative approach of VC-ALD for large (SW silicon) and small (LJ argon) thermal conductivity alloys for perturbative and large disorder. While the computational studies discussed above were limited to VC-ALD because of ab initio calcualtion costs, we use computationally cheap empirical potentials to include disorder explicitly. The effect of bond and mass disorder was investigated computationally by Skye and Schelling for Si/Ge⁴⁴, where it was shown that mass disorder is the dominant scattering mechanism. In this work we consider only mass disorder.

C. Calculation and Simulation Details

Perfect and explicitly disordered lattice supercells are generated with atomic positions based on LJ argon’s FCC ($n = 4$) and silicon’s diamond-FCC ($n = 8$) crystal structure, where n is the number of atoms in the unit cell. Supercells are built cubically with size N_0 , where N_0 refers to the number of repetitions of the unit cell in all 3 spatial directions. Supercells up to size $N_0 = 12$ (6096 atoms) are used for the LJ argon calculations. For SW silicon, $N_0 \leq 10$ (SW silicon, 8000 atoms) are used for the MD-based NMD methods, and $N_0 \leq 42$ for MD-based GK and VC-ALD (see Appendix ??).

Disorder is created by randomly specifying the masses of the atoms on the lattice. The composition of the lattices is labeled by $m_{1-c}^i m_c^j$, where $m^i = 1$ and $m^j = 3$ in LJ units for argon and $m^i = m_{Si}$ and $m^j = 2.6m_{Si}$

for SW silicon and “heavy silicon” (mass of germanium). For SW silicon, the lattice constant $a = 5.43\text{\AA}$ is used for all calculations, which brings the GK thermal conductivity predictions at 300K^{26,27} into better agreement with VC-ALD²⁸ for bulk SW silicon. For LJ argon, supercells are built using the zero-pressure finite-temperature lattice constants, which are $a = 1.556$ ($T=10$ K) and $a = 1.580$ ($T=40$ K) in LJ units.²⁵ For LJ argon, the variation of lattice constant with composition is small and ignored.(cite) The amorphous LJ phase was created by liquifying the crystal and instantly quenching by removing all kinetic energy. The resulting structure was then energy minimized and annealed in an NPT ensemble at zero pressure and $T = 10$ K.(cite lammps)) The effective zero-pressure lattice constant of the amorphous phase at $T=10$ K, based on the atomic density, is slightly larger ($a = 1.585$).²⁵

The MD simulations were performed by equilibrating in a NVT (constant number of atoms N, volume V, and temperature T) ensemble before calculating atomic positions and velocities in a NVE (constant number of atoms N, volume V and energy E) ensemble.(cite) Statistical averaging is accomplished using 10 simulations with different initial conditions. MD simulation time steps of 4.285 and 0.5 fs were used for LJ argon and SW silicon. For the NMD method (Section), the atomic positions and velocities were sampled at a rate dictated by the highest vibrational frequencies in the system, which can be estimated from harmonic lattice dynamics calcualtions (Section). For the GK method, the heat current was computed every 10 time steps. It is important to note that the same atomic trajectories are used for the NMD and GK methods.

III. VIBRATIONAL MODE PROPERTIES IN ALLOY SYSTEMS

A. VC and Gamma DOS

In this section, we examine the effect of explicit disorder by computing the density of states (DOS, $D(\omega)$) for vibrational modes of disordered lattice supercells and their equivalent VCs. The frequencies are computed using harmonic lattice dynamics calculations with the package GULP.²⁹ For the VC, the allowed wavevectors are set by N_0 . For the disordered supercells, the only allowed wavevector is the gamma-point (i.e., $\kappa = 0$). The DOS for the VC and the explicitly disordered supercells (referred to herein as Gamma) are shown in Fig. . The VC and Gamma DOS agree at low frequencies, where the Debye approximation predicts $DOS \propto \omega^2$.(cite) The Debye approximation underpredicts the the DOS at moderate frequency, which is due to the non-linear dispersion.(cite Mermin)

SiGe DOS predictions

The increasing lattice mass with increasing concentration for the VC reduces the frequencies. The increasing

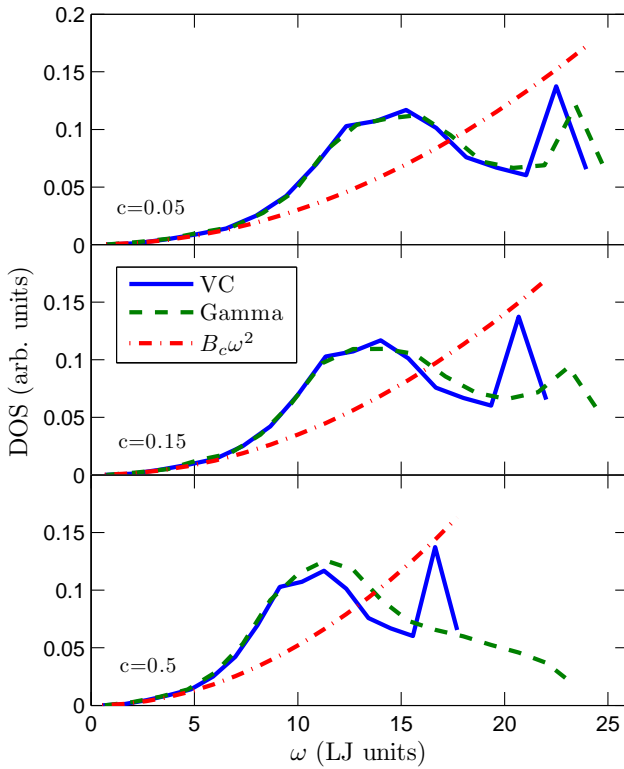


FIG. 2: Density of states (DOS) for modes calculated using the LJ FCC VC versus an explicitly mass disordered LJ FCC supercell (labeled Gamma) with varying mass concentration c (Section). VC and Gamma show similar low frequency behavior for all c . For increasing c , the frequencies of both VC and Gamma decrease, while the high frequency DOS for Gamma spreads and reaches up to a higher maximum frequency because of the explicit disorder. The size of these supercells is $N_0 = 12$ (see Section).

lattice mass for the Gamma modes also reduces the frequencies. The effect of explicit disorder is seen at high frequencies by a broadening and a shift of the DOS to higher frequencies because of the explicit use of light atoms in the supercell. Duda et al observed similar high-frequency broadening effects in model LJ alloys.³⁰ Similar agreement at low frequencies was found in *ab initio* predictions for Si_cGe_{1-c},⁸ while Bouchard showed similar continuous behavior at low frequency for a-Si_cGe_{1-c}.³¹

B. Dispersion and Group Velocity

1. From Virtual Crystal

The group velocity vector in a VC is the gradient of the dispersion curves,

$$v_{g,n}(\kappa) = \frac{\partial\omega(\kappa)}{\partial\kappa}. \quad (3)$$

We calculate the group velocities for the VC using finite differences and quasi-harmonic lattice dynamics.³²

Except for the three acoustic branches (2 transverse, 1 longitudinal), there is not an accepted method to predict the effective group velocity of a vibrational mode in a disordered system, although there have been attempts.^{19,24,30,33,34} In the Cahill-Pohl (CP) model, the group velocity of all disordered modes is the sound speed, v_s .²⁴ Dispersion for a model disordered 1D system demonstrated the reduction of the frequency-dependent group velocities due to the zone-folding effect.³⁰ By predicting the plane-wave character of vibrational modes, the structure factor of explicitly disordered modes can be used to assess the applicability of the VC approximation.(cite)

2. From Structure Factor of Gamma Modes

Calculating the structure factor of Gamma modes is a method to test for the plane-wave character of disordered modes at a particular wavevector and polarization.^{20,35} Feldman et al used the structure factor to predict an effective dispersion for a model of a-Si, but did not predict group velocities.²⁰ Volz and Chen used the dynamic structure factor to predict the dispersion of crystalline SW Si using MD simulation.³⁶

The structure factor is defined as³⁵

$$S^{L,T}(\kappa) = \sum_{\nu} E^{L,T}(\kappa=0) \delta(\omega - \omega(\kappa=0)), \quad (4)$$

where E^T refers to transverse polarization and is defined as

$$E^L(\kappa=0) = \left| \sum_{l,b} \hat{\kappa} \cdot e(\kappa=0 \alpha) \exp[i\kappa \cdot \mathbf{r}_0(l_b)] \right|^2 \quad (5)$$

and E^L refers to longitudinal polarization and is defined as

$$E^T(\kappa=0) = \left| \sum_{l,b} \hat{\kappa} \times e(\kappa=0 \alpha) \exp[i\kappa \cdot \mathbf{r}_0(l_b)] \right|^2. \quad (6)$$

Here, $\mathbf{r}_0(l_b)$ refers to the atomic positions of the mass disordered atoms in the supercells, which are still spatially ordered. Explicit disorder is accounted for in the mode frequencies $\omega(\kappa=0)$ and eigenvectors $e(\kappa=0 \alpha)$, which are calculated with $\kappa = 0$. The structure factors for LJ argon alloys are plotted in Fig. for wavevectors allowed by the VC.

Physically, $S^{L,T}(\kappa)$ represents the frequency spectrum required to create a wavepacket with a well-defined wavevector and polarization.^{20,35} The details of the calculation are given in Appendix . For a perfect lattice, the structure factor peaks are delta functions centered at the phonon mode frequencies, indicating they are pure

plane-waves. With increasing disorder, the structure factor spreads in width in Fig. , particularly at high frequencies because the modes are no longer pure plane-waves. The spectral mode factors $E^{L,T}(\kappa=0)$ represent the plane-wave character of any given mode $\omega(\kappa=0)$. We find that individual modes cannot be assigned a unique wavevector using $E^{L,T}(\kappa=0)$, in agreement with similar results for a-Si.(cite)

From Fig. , an effective dispersion can be extracted by locating the peaks in the structure factors at neighboring VC wavevectors, where the effects of polarization, virtual mass, and anisotropic dispersion can be observed. As the lattice VC mass becomes larger, the peaks in the structure factor shift to lower frequencies. The peaks in the structure factor are at slightly higher frequencies than the VC predicted frequencies by up to only %. Similarly, good agreement is found with the disordered SW silicon lattices (not shown), while the structure factors are more complicated because of the optical modes. Because of this good agreement, we use the group velocities predicted by the VC dispersion for both LJ argon and SW silicon with the VC-NMD and VC-ALD calculations for consistency and simplicity. We will examine the validity of this choice of group velocity in Section . Well-defined peaks (see Appendix) at all wavevectors are most likely due to the lattice structure of the disordered systems studied in this work. Typically, the structure factor for amorphous materials has well-defined peaks only for small wavevector.^{20,35}

C. Lifetimes

1. From VC-NMD and Gamma-NMD

As an alternative to the VC-ALD models for predicting phonon lifetimes, which are discussed in the next section, we first use the normal mode decomposition (NMD) method.^{37,38} NMD maps the atomic trajectories (positions and velocities) of atoms in an MD simulation onto the vibrational normal mode coordinates,(cite)

$$q(\kappa; t) = \sum_{\alpha, b, l}^{3, n, N} \sqrt{\frac{m_b}{N}} u_\alpha(b; t) e^*(\kappa \cdot \dot{r}_\alpha(b; t)) \quad (7)$$

and

$$\dot{q}(\kappa; t) = \sum_{\alpha, b, l}^{3, n, N} \sqrt{\frac{m_b}{N}} \dot{u}_\alpha(b; t) e^*(\kappa \cdot \dot{r}_\alpha(b; t)) \exp[i\kappa \cdot \mathbf{r}_0(b)]. \quad (8)$$

where $\mathbf{r}_0(b)$ are the equilibrium positions of the atoms in the b th unit cell of the lattice supercell under the VC approximation. The total energy of a given vibrational mode is

$$E(\kappa; t) = \frac{\omega(\kappa)}{2} q(\kappa; t)^* q(\kappa; t) + \frac{1}{2} \dot{q}(\kappa; t)^* \dot{q}(\kappa; t) \quad (9)$$

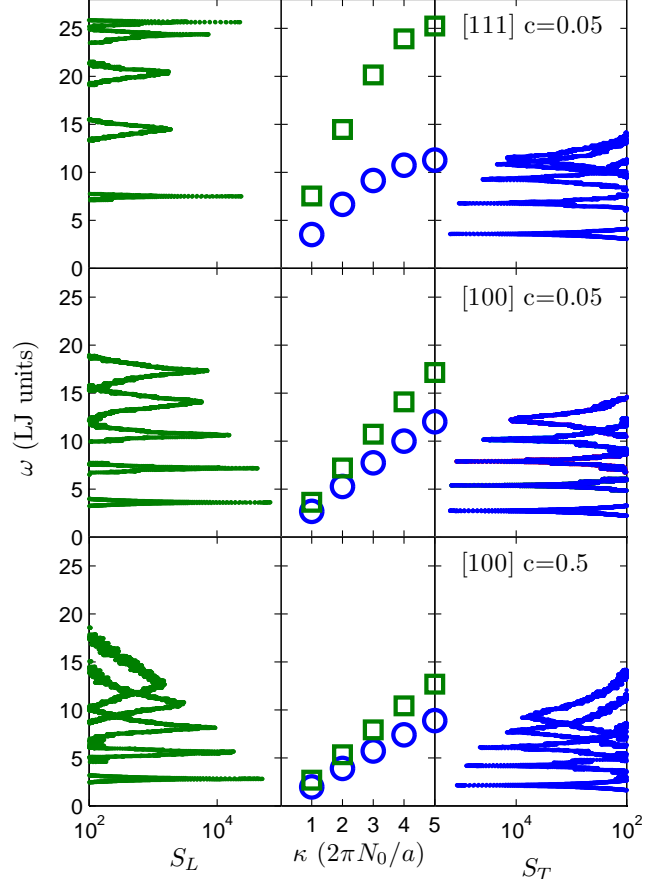


FIG. 3: Left and Right Panels: The structure factor for longitudinal (S_L) and transverse (S_T) polarizations along high symmetry directions ([100], [110] where $\kappa = \pi/a[100]$ and a is the lattice constant) of the mass disordered LJ FCC supercells ($c = 0.05, 0.5$). For increasing mass disorder c , there is a decrease in the center of the peaks and an increase in the peak linewidths. Center Panel: The VC predicted dispersion at the same wavectors used to calculate $S_{L,T}$.

We perform NMD using the frequencies and eigenvectors from both the VC ($\omega(\kappa)$, $e(\kappa \cdot \dot{r}_\alpha)$) and the Gamma supercell ($\omega(\kappa=0)$, $e(\kappa=0 \cdot \dot{r}_\alpha)$). The trajectories from these MD simulations are also used in the GK method (Section).

The normal vibrational mode lifetime is predicted using

$$\tau(\kappa) = \int_0^{\infty} \frac{E(\kappa; t) E(\kappa; 0)}{\langle E(\kappa; 0) E(\kappa; 0) \rangle} dt, \quad (10)$$

where the upper integration limit is set by the specifications of the MD simulation.(cite) This method for predicting lifetimes is able to handle the more complex behavior of the VC-NMD energy autocorrelations due to the disorder, which generally follow exponential decay (see Appendix B). This choice is an approximation which also makes it difficult to predict a phonon frequency, so

we use the VC predicted frequency for all VC-NMD predictions to compare with VC-ALD (Section).

The lifetimes predicted using VC-NMD and Gamma-NMD are shown in Fig. for LJ argon alloys. The range of frequencies of the modes for VC-NMD and Gamma-NMD differ slightly which is due to differences in the DOS (Fig.). For small intervals of frequency, there are a wider range of predicted lifetimes for Gamma-NMD. This is because there is no symmetry averaging of the mode properties, which is possible for the VC. Lifetimes predicted by both VC-NMD and Gamma-NMD show scalings with frequency of ω^{-2} at low frequency and ω^{-4} and even faster for mid-range frequencies (Fig.). In general, the lifetimes predicted by both VC-NMD and Gamma-NMD are larger than the Ioffe-Regel (IR) limit,³⁹

$$\tau = \frac{2\pi}{\omega}. \quad (11)$$

The physical interpretation of the IR limit is that of a mode which scatters in a time equal to its oscillation period, which seems to be a good lower-limit for the lifetimes predicted by VC-NMD and Gamma-NMD for LJ argon (Fig.) and VC-NMD for SW silicon (Fig. (a)).

The behavior at the highest frequencies, where $\tau \propto \text{constant}$, is seen for both VC-NMD and Gamma-NMD, except at $c = 0.5$ for VC-NMD. Since the existence of this characteristic (thought not exactly minimum) lifetime for LJ argon is demonstrated by both VC-NMD and Gamma-NMD, it is physically meaningful. There is, however, no theoretical prediction of this high-frequency behavior of the mode lifetime.^{24,40,48} This plateau in lifetimes at high-frequency is not seen for VC-NMD and SW silicon (Fig.).

Overall, good agreement is seen in the predicted lifetimes from VC-NMD and Gamma-NMD both in magnitude and trends. The use of the VC normal modes is an approximation which becomes worse as the concentration is increased (Appendix). The only approximation associated with Gamma-NMD is the use of the harmonic lattice dynamics predicted frequencies and eigenvectors to map the atomic trajectories from the fully anharmonic MD simulations. (cite) Based on the good agreement with Gamma-NMD, the lifetimes predicted by VC-NMD are used along with the VC predicted group velocities to predict thermal conductivity in Section .

2. From VC-ALD

Assuming intrinsic and disorder scattering mechanisms to operate independently, the effective phonon lifetime can be found using Matthiessen's rule(cite),

$$\frac{1}{\tau(\kappa)} = \frac{1}{\tau_{p-p}(\kappa)} + \frac{1}{\tau_{p-d}(\kappa)}, \quad (12)$$

where $\tau_{p-p}(\kappa)$ accounts for intrinsic phonon-phonon scattering and $\tau_{p-d}(\kappa)$ accounts for defect scattering.

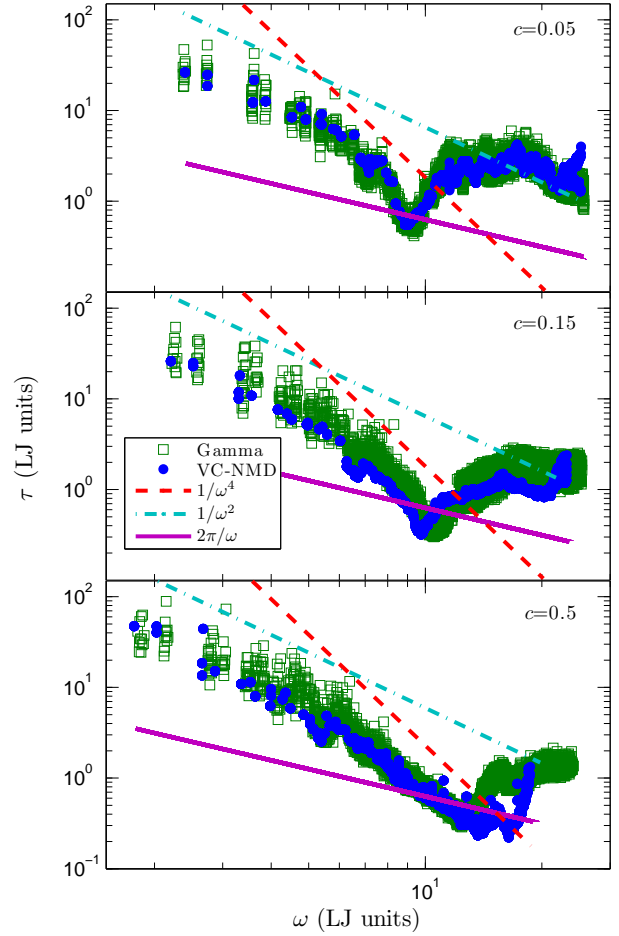


FIG. 4: Lifetimes predicted using VC-NMD and Gamma NMD from MD simulations of mass disordered lattice supercells (Section). Both ω^{-2} and ω^{-4} scalings can be observed at low frequencies, which are predicted by the perturbative models used for VC-ALD (Section). For both VC-NMD and Gamma NMD, most mode lifetimes are greater than the Ioffe-Regel limit $\tau = 2\pi/\omega$.³⁹ While there is more “noise” in the Gamma mode data (Section), the lifetime magnitudes and trends agree well, an important consideration when comparing VC-NMD and VC-ALD in Fig. .

Phonon-phonon scattering ($\tau_{p-p}(\kappa)$) is typically treated using anharmonic perturbation theory (ALD) including only three-phonon processes.^{3,8,38} It has been demonstrated that the effects of higher order phonon processes become important at high temperatures (see Section).^{38,41} In this work, the intrinsic phonon lifetimes $\tau(\kappa)_{p-p}$ are predicted using the method described in³⁸, with all classical expressions to remain consistent with the classical MD-based methods NMD and GK.

Using harmonic perturbation theory, Tamura derives a general expression for mass point defect scattering.¹⁴ By considering the symmetry properties of the FCC lattices

considered in this work (Section), it can be shown that¹⁴

$$1/\tau_d(\boldsymbol{\nu}) = \frac{\pi}{2} g_2 \omega^2(\boldsymbol{\nu}) D(\omega), \quad (13)$$

where $D(\omega)$ is the density of states (Section) and $g_n = \sum_{\mu} c^{\mu} (1 - m^{\mu}/\bar{m}^{\mu})^n$. Here, c^{μ} is the concentration, m^{μ} is the mass of the μ -th species and \bar{m}^{μ} is the average mass. Bond disorder can be accounted for using a similar expression with an average atomic radius or suitable scattering cross-section.^{42,43} For the binary LJ argon and SW silicon alloys considered, there is one atom type in the unit cell with $\mu = i, j$, so that the alloying atom labeled by m_{1-c}^i can be considered to be an “isotope” of atom labeled m_c^j . This convention is appropriate because of the perturbative approach used to derive Eq. (), while we consider large disorder.¹⁴ To calculate the disordered lifetimes $\tau(\boldsymbol{\nu})_d$ (Eq.), it is necessary to broaden the δ function using a Lorentzian function.[1] footnote[1] For all calculations, the Lorentzian was broadened using a value of $100\delta_{\omega,\text{avg}}$ (Section). For the system sizes here, the results do not differ significantly if this broadening value is varied manually or by increasing system size (N_0).

At low frequencies where the density of states is Debye-like ($D(\omega) \propto \omega^2$, Fig.), $\tau_{p-p}(\boldsymbol{\nu})$ follows a scaling due to both normal ($B_1 \omega^{-2}$) and umklapp ($B_2 \omega^{-2}$) 3-phonon scattering processes, where the constants B_1 and B_2 are typically fit to experimental data.(cite) From Fig.s and , the scaling $\tau \propto \omega^{-2}$ can be observed in both the VC-NMD, Gamma-NMD and VC-ALD predicted results. Under the Debye-approximation , the phonon scattering due to mass point-defects is given by $A\omega^{-4}$, where A is a constant related to the unit cell volume, branch-averaged group velocity, and disorder coupling strength ($g_2(b)$ in Eq. above). The frequency dependence (ω^4) is the same as Rayleigh scattering, which is valid at low frequency and observed in both the NMD (Fig.) and ALD (Fig.) predicted lifetimes. VC-ALD does not predict the behavior of the lifetimes at high frequency for LJ argon, $\tau \propto \text{constant}$ (Fig.), where VC-NMD and Gamma-NMD do (Fig.). The thermal conductivity of LJ argon alloys is dominated by high frequency modes (Fig.)(cite). For SW silicon alloys, the thermal conductivity is dominated by low-frequency modes, while the high frequency discrepancy is not observed using VC-NMD and VC-ALD (Fig.).

The Tamura theory was developed to predict the reduction of lifetimes in isotopic Ge, which is only perturbatively disordered. The terms g_n are coupling terms which define the strength of the disorder and the importance of n-order interactions in the Tamura theory. With increasing disorder, the importance of higher-order ($n > 2$) terms in the Tamura theory can be estimated by $g_n|I(\omega)|^{n-2}/g_{n-1}$, where $I(\omega)$ is related to the DOS.¹⁴

For isotopically-disordered Ge, the higher-order contributions $g_n|I(\omega)|^{n-2}/g_{n-1}$ were estimated to be negligible for all frequencies.¹⁴ For LJ argon and the large concentrations and mass ratios considered in this work,

the terms $g_n|I(\omega)|^{n-2}/g_{n-1}$ are order 1 and larger at high frequencies. It is possible that higher-order interactions in the Tamura theory is responsible for the discrepancy of the lifetimes predicted by VC-NMD and Gamma-NMD versus VC-ALD at high frequency. For SW silicon alloys the higher-order terms are also large, while good agreement is observed at high frequencies for VC-NMD and VC-ALD (Fig.).

D. Diffusivities

In the classical harmonic limit, where the specific heat $c_p(\boldsymbol{\nu}) = k_B$, a vibrational mode’s contribution to thermal conductivity is determined by the mode thermal diffusivity. For phonons, the thermal diffusivity is

$$D_{ph,n}(\boldsymbol{\nu}) = \mathbf{v}_{g,n}(\boldsymbol{\nu}) \tau(\boldsymbol{\nu}). \quad (14)$$

For VC-NMD and VC-ALD, $\mathbf{v}_{g,n}(\boldsymbol{\nu})$ is calculated from the VC dispersion (Section) so any differences in thermal diffusivity comes from the predicted lifetimes. The lower limit for phonon thermal diffusivity is $D_{ph,n}(\boldsymbol{\nu}) \approx 0$ since the group velocities can approach 0 for modes such as optical and those near the Brioullin zone boundaries.(cite)

In disordered systems, modes can transport heat by harmonic coupling due to disorder in the Allen-Feldman (AF) theory of diffusons.¹⁶ In the high-scatter (HS) limit,(cite) the AF diffusivity of each mode is

$$D_{AF,HS} = \frac{1}{3} v_s a, \quad (15)$$

and the AF thermal conductivity prediction is

$$k_{AF,HS} = \frac{k_B}{V_b} b v_s a, \quad (16)$$

where V_b is the volume of the unit cell, v_s is the branch-averaged sound speed, and a is the lattice constant.²⁴ The Cahill-Pohl (CP) HS limit differs from the AF,HS model by a factor of approximately %20.²⁴ The physical interpretation is all vibrational modes transport heat at the sound speed and scatter with a mean free path of the lattice spacing.

As seen in Fig. and , VC-NMD and VC-ALD predict a significant number of modes with $D_{ph}(\boldsymbol{\nu}) < D_{AF,HS}$ for both LJ argon and SW silicon. This can lead to an underprediction of the total thermal conductivity. The diffusivity of these modes can be adjusted such that any mode with $D_{ph} < D_{AF,HS}$ is given $D_{ph} = D_{AF,HS}$. The result of this adjustment, referred to as VC-NMD* and VC-ALD*, is examined in the thermal conductivity predictions in Section .

While AF,HS model assumes a mode-independent thermal diffusivity, the AF theory is capable of predicting the mode specific diffusivities.^{5,5,20,47} In the harmonic AF theory, mode diffusivities typically diverge as $\omega \rightarrow 0$ because the vibrational modes are long-wavelength plane waves that weakly scattered by the disorder.^{45,46} The

mode-specific thermal diffusivities for the LJ argon amorphous phase are shown in Fig. . Modes with significant contribution to thermal transport can be modeled using a mode-independent diffusivity of approximately $D_{AF,HS}$. Also shown are the AF predicted thermal diffusivities for the explicitly disordered superlattice and $c = 0.5$. While the AF theory is divergent in the low-frequency limit for lattices, the finite system size limits the thermal diffusivities of the lowest frequencies (Fig). The thermal diffusivity of all modes in the explicitly disordered lattice supercell are larger than $D_{AF,HS}$, except at the highest frequencies where they tend to zero as in the amorphous phase (Fig).(cite) This result supports the plausible lower-bound, $D_{ph} \geq D_{AF,HS}$.

Predictions from model disordered systems demonstrates the existence of a plateau of the thermal diffusivity, which is consistent with the minimum phonon mean-free path hypothesis.⁴⁹ A minimum vibrational mean free path is used in most models of thermal transport in disordered materials.^{24,40,48} However, the concept of a vibrational mean free path is only valid for low-frequency propagating modes in disordered systems.²⁰ The more fundamental property is the vibrational mode lifetime.³⁹

For disordered systems it is only possible to assign a unique lifetime and group velocity to a vibrational mode only in the low-frequency, propagating limit.^{20,50} This implies that the VC predicted group velocities, particularly for $v_g(\kappa) \ll v_s$, are an underprediction of the representative velocity scale for the thermal diffusivity of high-frequency modes in the disordered lattice.

VC-NMD predicts lifetimes which are generally larger than the IR limit (Eq.) for both LJ argon and SW silicon alloys. VC-ALD predicts essentially monotonically decreasing lifetimes with increasing frequency for both LJ argon and SW silicon (Fig.). Because VC-NMD and VC-ALD use the same predictions for $v_g(\kappa)$, the phonon mode diffusivities $D_{ph}(\kappa)$ are underpredicted for VC-ALD compared to VC-NMD for LJ argon alloys (Fig). There are thus 2 underpredictions to consider when predicting the thermal conductivities in predictions: underprediction of the thermal diffusivity assuming the VC group velocities for VC-NMD and VC-ALD, and the underprediction of the mode lifetimes for LJ argon alloys by the VC-ALD perturbative models.

IV. THERMAL CONDUCTIVITY PREDICTIONS

The thermal conductivity can be predicted using the mode properties predicted by the VC-NMD and VC-ALD methods. Given the discussion of the preceeding section, it is necessary to implement a third method for predicting thermal conudctivity. We choose the equilibrium MD-based green-kubo (GK) method.(cite) This method does not predict any mode-specific properties, and is thus a system-level prediction. Thermal conductivity predicted by GK has been shown to capture the effects of what-

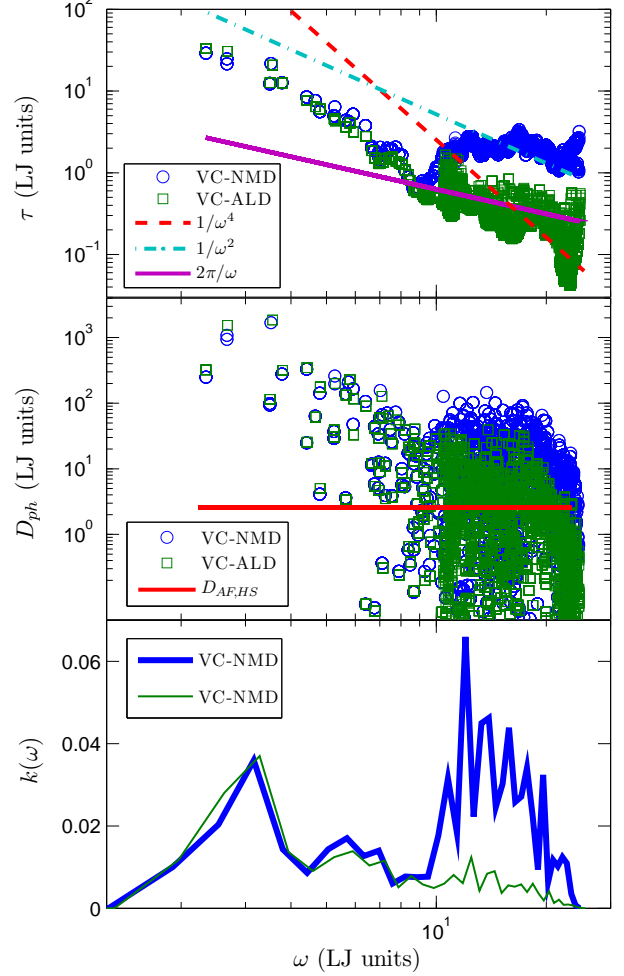


FIG. 5: (a) predicted lifetimes for VC modes using VC-NMD and VC-ALD for LJ argon. (b) predicted VC mode thermal diffusivities, compared to the AF,HS limit. (c) the thermal conductivity frequency spectrum, which is peaked at high frequency, in contrast to SW silicon (Fig.).

ever scattering meachanisms are present in the MD simulation without any assumptions (other than those that come with the classical nature of the MD siulation).(cite) Details of the GK and MD simulations are given in Appendix . For LJ argon, bulk thermal conductivity predictions are made for VC-NMD, VC-ALD and GK (Fig.). For SW silicon, bulk thermal conductivity predictions can only be made for VC-ALD and GK because of the limited system size used for VC-NMD (see Appendix).

For LJ argon, VC-NMD and VC-ALD underpredict the thermal conductivity compared to GK. The underprediction is only modest for VC-NMD, on the order of 20% or less for all c . By adjusting the mode diffusivity as suggested in Section , the thermal conductivtiy predicted by VC-NMD* is brought into agreement with GK by approximately 10% or less for all c . Combined with

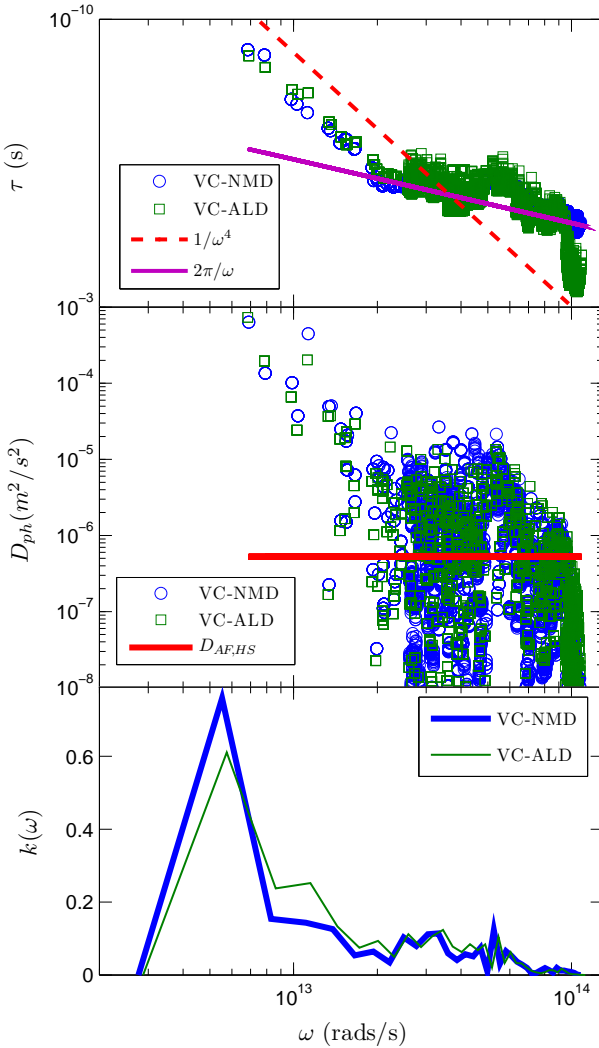


FIG. 6: (a) predicted lifetimes for VC modes using VC-NMD and VC-ALD for SW silicon. (b) predicted VC mode thermal diffusivities, compared to the AF,HS limit. (c) the thermal conductivity frequency spectrum, which is peaked at low frequency, in contrast to LJ argon (Fig.).

the high-scatter limit, the VC-NMD predicted thermal diffusivities are a fair representation of the explicitly disordered modes present in the MD simulation when.

The VC-ALD method underpredicts the thermal conductivity of LJ argon alloys, where the underprediction is worst for $c = 0.05$, $k_{VC-ALD}/k_{GK} = 0.56$ (error bars are on the order of the large symbol sizes in Fig.). By applying the high-scatter limit adjustment VC-ALD*, the thermal conductivities are brought into marginally better agreement, worst for $c = 0.05$, $k_{VC-ALD^*}/k_{GK} = 0.65$.

The failure of the VC-ALD method can be demonstrated further by moving to higher temperature $T = 40$ K in Fig. . The beginning breakdown of the intrinsic phonon-phonon ($\tau_{p-p}(\omega)$) scattering model can be observed for $c = 0.0$ at $T = 40$ K (Fig.), where ALD begins to overpredict compared to GK. This can be explained

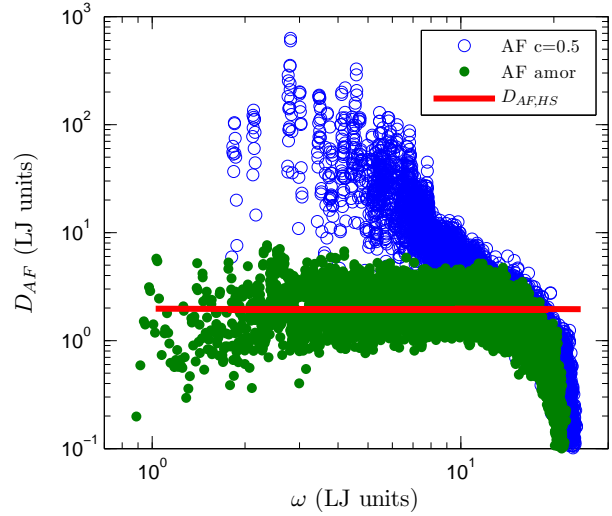


FIG. 7: AF theory predictions of disordered mode thermal diffusivities for LJ argon disordered lattice supercell and amorphous phase. The mode thermal diffusivities predicted for the disordered lattice supercell are all finite, except at the highest frequency where they tend to 0 as in the amorphous phase.

by the emerging importance of higher order ($n > 3$) n-phonon process at high temperatures.³⁸ While the VC-ALD method begins to overpredict for $c = 0.0$ at elevated temperature, it continues to underpredict for the alloys $c \geq 0.05$. In fact, the thermal conductivity predictions for VC-ALD are at or slightly below the high-scatter limit $k_{AF,HS}$.

The VC-ALD method fails to accurately predict the high-frequency mode thermal diffusivities for LJ argon alloys, which can be seen in the thermal conductivity spectrum Fig. .(cite) Since the group velocities for VC-NMD and VC-ALD, this underprediction of the high-frequency thermal diffusivities is due to the underprediction of the high-frequency mode lifetimes (Fig.). At $T=40$ K, the thermal conductivity of the diffusivity adjusted VC-ALD* is only marginally improved compared to GK.

For SW silicon, the thermal conductivities predicted by VC-ALD and GK are in better agreement, even without the adjustment VC-ALD*. VC-ALD actually overpredicts by roughly 20% for $c \geq 0.05$ compared to GK. The overprediction of thermal conductivity by VC-ALD may be related to the role of disorder in the ALD calculation.^{8,38} While Garg et al found an overprediction of VC-ALD compared to experiment by a factor of two, the overprediction we observe in this work for SW silicon alloys is not as drastic. For SW silicon alloys, the VC-ALD* adjustment increases the result from VC-ALD by about 1% because the contribution from high-frequency modes is only a few percent (Fig.).

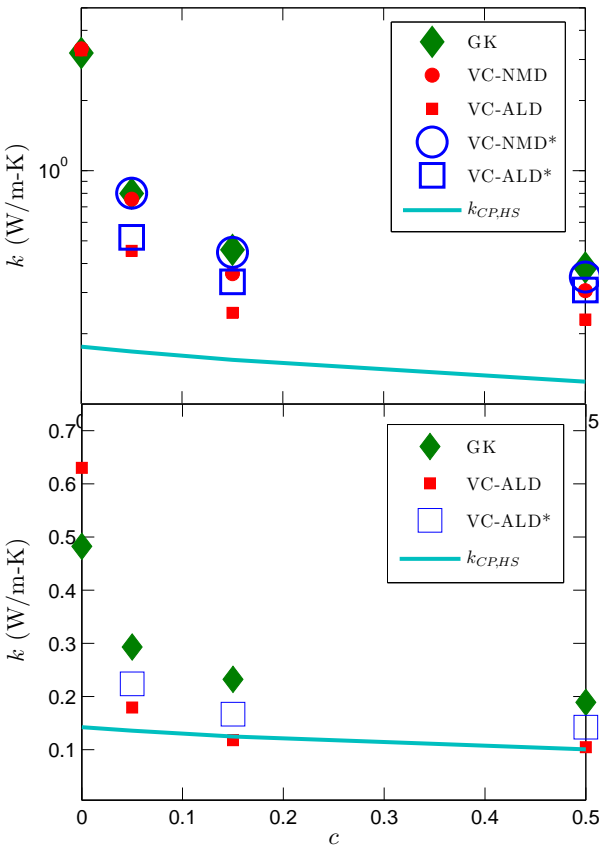


FIG. 8: (a) thermal conductivity predictions for LJ argon alloys at $T=10\text{K}$ using the VC-NMD, VC-ALD, and GK methods. (b) thermal conductivity predictions at $T=40\text{K}$.

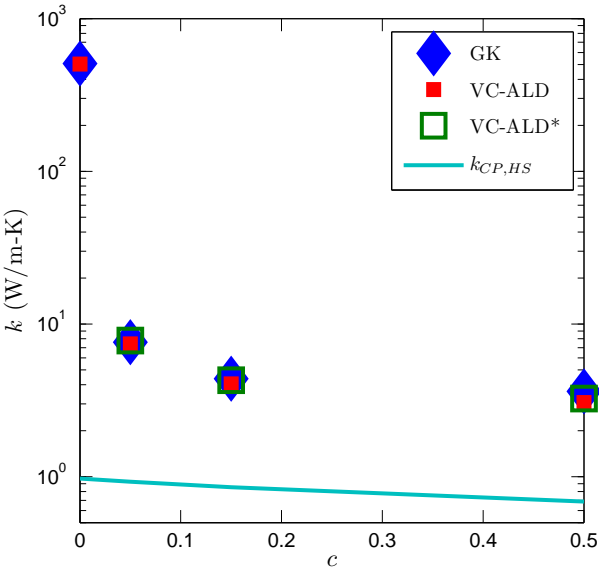


FIG. 9:

V. DISCUSSION

The LJ argon and SW silicon alloys studied in this work have different ranges of phonon frequencies, lifetimes, group velocities and total thermal conductivity. For bulk silicon(cite), the thermal conductivity is dominated by low-frequency modes(cite), which is also true for bulk and alloyed SW silicon (Fig.).(cite) For SW silicon, VC-ALD predicts thermal conductivities in reasonably good agreement with the explicitly disordered GK method (Fig.). For LJ argon, VC-ALD underpredicts the high-frequency phonon lifetimes (Fig.), leading to an underprediction of thermal conductivity when compared to the explicitly disordered methods VC-NMD and GK (Section).

The results for SW silicon and LJ argon alloys suggest that the thermal modeling of ordered and disordered lattices can be separated into two broad groups: low- and high-frequency dominated materials.(cite) Materials dominated by low-frequency modes tend to have high thermal conductivities, which is due to their large group velocities and long lifetimes. (cite) These low-frequency modes follow closely the scalings predicted by the perturbative VC-ALD models, which are valid at low-frequencies.

LJ argon is a material which is dominated by high-frequency modes, even for the bulk (Fig.). This high-frequency range is where the perturbative VC-ALD models underpredict the mode lifetimes (Fig.), and also where the higher-order terms in the Tamura theory are predicted to be non-negligible (Section). While the high-order terms in the Tamura theory are also predicted to be non-negligible for SW silicon, this does not affect the thermal conductivity predictions significantly. Even if there was a discrepancy at high-frequency these modes are unimportant to thermal transport in SW silicon (Fig.). This is also true for the thermal conductivity spectrum of SiGe alloys from first-principles predictions⁸ and experimental measurements.^{21?}?²² and first-principles predictions^{7,8} this is also true for SiGe alloys and isotopic GaN. For example, the thermal conductivity of SiGe alloys exceeds the high-scatter limit by more than an order of magnitude at room temperature for all compositions.

Resolution of the breakdown of the perturbative VC-ALD models for LJ argon is achieved by considering the thermal diffusivity of vibrational modes in the AF theory. A simple correction to the VC approximation can be made by considering a high-scatter limit for the mode specific thermal diffusivity (Section, Fig.). This high-scatter limit is physically interpreted as vibrational modes propagating at the sound speed a distance of the lattice constant (Section Fig.). However, the concept of a vibrational mean free path in a disordered system is only valid at low-frequencies.^{20,50} For disordered vibrations, the lifetime and thermal diffusivity are the fundamental quantities. The VC approximation underpredicts the mode thermal diffusivity due to disorder because the group velocities $v_g(\kappa)$ can approach zero (Sec-

tion), though this is a small effect compared to the underprediction of the lifetimes by VC-ALD.

For LJ argon, it is possible that the VC group velocities are an over-prediction for modes in a given interval of frequency, an effect which is compensated for by a small under-prediction of the lifetimes in the same interval of frequency when compared to Gamma-NMD (Fig.). The VC-NMD predicted mode lifetimes and thermal diffusivity adjusted VC-NMD*, predict thermal conductivities in good agreement with the MD-based GK method (Fig.). Based on the thermal conductivity predictions for VC-NMD* and the well-defined peaks in the structure factors (Fig.), the reduction of group velocities in disordered lattices due to zone folding seems to underpredict the group velocity of moderate to high frequency modes.³⁰

The predictions using VC-NMD, VC-ALD demonstrate the importance of explicit disorder modeling in “soft” systems and possible underprediction of the thermal properties.³

VI. SUMMARY

The concept of simple alloying is at the forefront of the effort to control or minimize the thermal conductivity of semiconducting and thermoelectric materials (cite SiGe nanoporous, PbTe) Results in this work suggest that the lower limit for the vibrational mode thermal diffusivity in alloys with thermal conductivities near the high-scatter limit is $(1/3)v_s a$. Such materials include the thermoelectric PbTe, particularly at the high operating temperatures of thermoelectric energy generation.(cite) PbTe has a thermal conductivity in the mid-range of frequencies, placing it between SW silicon and LJ argon. The optical phonons in PbTe/PbSe alloys have been predicted to have group velocities as large as the acoustic branches, making PbTe/PbSe distinctly unique compared to SW silicon or LJ argon alloys.³ It is not clear what role the high-scatter limit of the mode-specific thermal diffusivity has in predictions for PbTe/PbSe alloys.

The results in this work support the idea of a minimum thermal diffusivity for the vibrations in disordered lattices.(cite) Although this minimum thermal diffusivity is usually interpreted as a minimum mean free path, we find that concept is not necessary for interpreting the results. The VC approximation provides a computationally cheap framework, which is essential for expensive but experimentally accurate *ab initio* methods for predicting thermal conductivity.(cite) The high-scatter limit of thermal diffusivity is more useful for examining the thermal transport in alloys under the framework of the VC approximation. The fundamental quantity is the mode lifetimes and the group velocity is an approximation, and expressed together as thermal diffusivity they can be interpreted in the presence of disorder.

Acknowledgments

This work was supported in part by a grant of computer time from the DOD High Performance Computing Modernization Program at the US Army Engineer Research and Development Center. We thank Jivtesh Garg, Zhiting Tian, Davide Donadio, Asad Hasan and Craig Maloney for helpful discussions.

Appendix A: Computational Cost

The key to incorporating the effects of disorder explicitly are the use of a large disordered supercells (Section). However, the methods used in this work scale differently with the size of the supercell considered. The calculations in this work are trivially parallelizable except the MD simulations⁵² and the eigenvalue solution of the Dynamical matrix (Section).²⁹ Efficient MD codes scale linearly with the number of atoms in the system N_a , making the GK method an efficient method for predicting thermal conductivity. However, the computational cost of using large supercells for MD simulation, particularly because of the large number of time steps required (on the order of $10^5 - 10^7$ depending on the system, time step used, etc (cite)), prohibit its use with typical *ab initio* methods such as plane-wave Density Functional Theory.(cite)

Both VC-NMD and VC-ALD require the eigenvalue solution of a Dynamical matrix of size $(3n, 3n)$ for each irreducible wavevector of the system size considered, which is negligible compared to the other caculations required for both of these methods.(cite) The Gamma-NMD (Section) and AF theory (Section) require the eigenvalue solution of a large Dynamical matrix $(3N_a, 3N_a)$, the solution of which scales as $(3N_a)^3$ (Section). The AF theory is limited to small supercells using ab initio calculations, making it difficult to asses finite-size effects (Section).

Using the VC-ALD method, the symmetries of the system can be used to drastically reduce the required computations, permitting its use with ab initio methods.^{11,38,53,54} For VC-ALD, the calculation of the intrinsic phonon lifetimes $\tau_{p-p}(\kappa_\nu)$ scales as n^4 ,³⁸ making calcualtions for large unit cells challenging.(cite) Compared to the calculation of the intrinsic phonon lifetimes, calculation of the defect lifetimes $\tau_d(\kappa_\nu)$ (Eq.) is negligible.

Appendix B: NMD using Non-Exact Normal Modes

The NMD method reuires the atomic positions and velocities from an MD simulation.(cite) The MD simulations are performed using the package LAMMPS.⁵² The lengths of the MD simulations were longer than 10 times the longest phonon lifetime in the system. These can be estimated a priori from the VC-ALD predicted phonon lifetimes. For LJ argon and SW silicon, the simulations were run using time steps of $dt = 0.002$ LJ units and

$dt = 0.0005 fs$ for 2^{20} and 2^{22} time steps and the atomic trajectories were sampled every 2^8 and 2^4 time steps, respectively. Ensemble averaging was performed using 10 independent initial randomized velocity distributions.

For a normal mode of the lattice supercell used for the MD simulations (Section), the autocorrelation of the total and kinetic normal mode energy are damped exponentials with a decay time $\tau(\kappa_\nu)$, the kinetic energy autocorrelation with a cosinusoidal oscillation frequency $2\omega(\kappa_\nu)$. (cite joe) When using the VC normal modes (Section) to map the MD simulation trajectories for the explicitly disordered lattice supercells (Section), the mode total and kinetic energy autocorrelation functions do not always follow simple functional forms. This can be illustrated by using spectral-NMD in the frequency domain, where artifacts such as multiple peaks in an isolated mode's energy spectrum (Φ) can be observed (see Fig). (cite) In the case of multiple peaks, the choice of which peak to fit to predict the phonon properties can be ambiguous. However, a lifetime can be predicted unambiguously using Eq. even with these multiple-peak artifacts, particularly because the autocorrelations are damped exponentially. This results is to be expected given that the atomic trajectories contain information about the lattice energy, which from general statistical physics principles will have exponential relaxation behavior in an equilibrium ensemble.^{55–57}

These artifacts are not surprising given two considerations: 1) the MD simulations contain explicit disorder which influences the atomic trajectories 2) the VC normal modes are not the exact normal modes and of the explicitly disordered system. Discrepancies have been observed previously when the exact normal modes of the system are not used. (cite SED) However, the lifetimes predicted using VC-NMD are in fairly good agreement with those calculated using Gamma-NMD (Fig.). Several studies have found good agreement for predictions of lifetimes and thermal conductivity using non-exact eigenvector mappings^{12,58} in a wide-range of materials and phonon scattering conditions.^{2,10,12,58,59} However, it is crucial that results using non-exact mappings are compared to as many alternative methods as possible. In this work, VC-NMD is compared to the other methods Gamma-NMD (Section), GK (Section), and VC-ALD (Section). It is important to remember that the VC normal modes are exact in the limit $c \rightarrow 0$. Use of the VC modes at large c pushes the limits of the approximation, but is useful for predicting an effective group velocity (Section).

Appendix C: Calculation of the Gamma Mode Structure Factors

To calculate $S^{L,T}(\omega)$ for a finite-size system, the delta function in Eq. (??) is broadened using a Lorentzian function with a full-width at half maximum $\Gamma_{FMHz} = \delta_{\omega,avg}$, where $\delta_{\omega,avg}$ is the average frequency spacing.

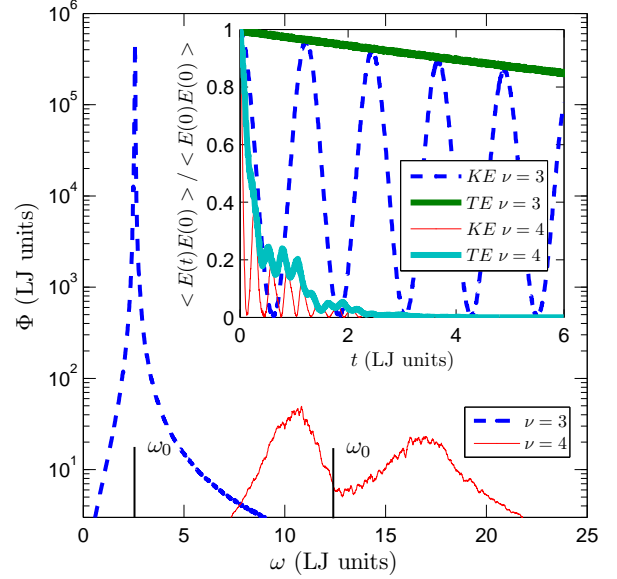


FIG. 10: The spectral energy density Φ of two modes (polarizations $\nu = 3, 4$ at wavevector $[0.2 \ 0 \ 0]$) calculated using VC-NMD for a mass disordered LJ FCC supercell ($N_0 = 8$ and $c = 0.5$, Section). The VC dispersion-predicted peaks are labeled by ω_0 . Inset: the same mode's energy (kinetic (KE) and total (TE)) autocorrelation functions. Note the additional harmonic effects in the KE and TE autocorrelation functions for $\nu = 4$ which are due to the double peaks in Φ . A mode lifetime can be extracted unambiguously using the integral of the TE autocorrelation function (Section).

Allen et al³⁵ demonstrated using a model of a-Si that the structure factor for large wavevector broadens so that the linewidth $\Gamma_{SF} > \omega$.³⁹ For the systems sizes studied, Γ_{SF} scale with the broadening factor Γ_{FMHW} for all peaks except those at high frequencies.

For the range of broadening factors considered ($\Gamma_{FMHW} = \delta_{\omega,avg}$ to $50\delta_{\omega,avg}$) the linewidths extracted for all c generally satisfy $\Gamma_{SF} > \omega$. For all broadening factors, the linewidths (inverse lifetimes, $\tau_{SF} = 1/2\Gamma_{SF}$) at high frequency are in better agreement with the lifetimes predicted by VC-NMD rather than VC-ALD, where generally $\tau > 2\pi/\omega$ (IR limit, Fig.).³⁹ This gives more justification for the use of the VC predicted group velocities for both VC-NMD and VC-ALD, even for large wavevector and c .

In general, the polarization of the eigenvectors $e_{\nu}^{(b)}$ will not be purely transverse or longitudinal along the reciprocal directions. Even for the simple LJ argon system, this can make it difficult to uniquely identify then different polarizations with the various peaks in the structure factors. For SW silicon, similar good agreement can be seen along the high symmetry directions for the acoustic branches, while the optical modes and more complicated polarizations are too difficult to identify in an automated way. In general, the acoustic branches can be identified, provided they are well separated in frequency from any

optical branches.^{20,58}

Appendix D: Finite Simulation-Size Scaling for Thermal Conductivity

To predict a bulk thermal conductivity, extrapolation is used by the following finite size scaling $1/k \propto 1/N_0$. For VC-NMD and VC-ALD, the validity of the finite-size scaling requires the low frequency modes in the finite system to be dominated by intrinsic scattering ($\tau(\kappa) \propto \omega(\kappa)^{-2}$, Section) and follow the Debye approximation with respect to $v_{g,n}$ (Section) and DOS $D(\omega(\kappa))$ (Section).^{10,11} For LJ argon, this requirement is satisfied for modest system sizes (for $N_0 = 6$ to 12) so that both VC-NMD and VC-ALD predictions can be extrapolated to a bulk value. For SW silicon, the thermal conductivity is dominated by low-frequency modes (Fig.). Because of this, large system sizes (up to $N_0 = 40$) are needed to satisfy the extrapolation requirements and only VC-ALD can be used.(cite) This demonstrates the computational efficiency of the VC-ALD method which is necessary when computationally expensive ab initio methods are used (Section).^{3,7,8,11}

System sizes of up to $N_0 = 38$ are required to predict converged thermal conductivity of SW silicon alloys. For Si modeled using the Tersoff potential, system sizes of up to 64000 atoms are required to observe converged values of thermal conductivity using the GK method.²⁷ We find that similar system sizes are also required for

For the GK method, smaller system sizes $N_0 \leq 12$ are used for the finite size extrapolation for LJ argon and SW silicon . The validity of this result can be explained in terms of a combination of effects which are specific to the MD simulations.¹¹ In fact, for $c = 0$ the GK results are independent of system size for $N_0 = 4$ to $N_0 = 12$ for LJ argon.

- ^{*} Electronic address: mcgaughey@cmu.edu
- ¹ B. Abeles, Phys. Rev. **131**, 19061911 (1963), URL <http://link.aps.org/doi/10.1103/PhysRev.131.1906>.
 - ² B. Qiu, H. Bao, G. Zhang, Y. Wu, and X. Ruan, Computational Materials Science **53**, 278 (2012), ISSN 0927-0256, URL <http://www.sciencedirect.com/science/article/pii/S0927025611004770>.
 - ⁴ J. M. Ziman, *Electrons and Phonons* (Oxford, New York, 2001).
 - ⁵ J. L. Feldman, M. D. Kluge, P. B. Allen, and F. Wooten, Physical Review B **48**, 1258912602 (1993).
 - ⁷ L. Lindsay, D. A. Broido, and T. L. Reinecke, Phys. Rev. Lett. **109**, 095901 (2012), URL <http://link.aps.org/doi/10.1103/PhysRevLett.109.095901>.
 - ⁸ J. Garg, N. Bonini, B. Kozinsky, and N. Marzari, Phys. Rev. Lett. **106**, 045901 (2011), URL <http://link.aps.org/doi/10.1103/PhysRevLett.106.045901>.
 - ⁹ T. Shiga, J. Shiomi, J. Ma, O. Delaire, T. Radzynski, A. Lusakowski, K. Esfarjani, and G. Chen, Phys. Rev. B **85**, 155203 (2012), URL <http://link.aps.org/doi/10.1103/PhysRevB.85.155203>.
 - ¹⁰ J. Shiomi, K. Esfarjani, and G. Chen, Physical Review B **84**, 104302 (2011).
 - ¹¹ K. Esfarjani, G. Chen, and H. T. Stokes, Physical Review B **84**, 085204 (2011).
 - ¹² N. d. Koker, Physical Review Letters **103**, 125902 (2009), URL <http://link.aps.org/abstract/PRL/v103/e125902>.
 - ¹³ H. Bao, B. Qiu, Y. Zhang, and X. Ruan, Journal of Quantitative Spectroscopy and Radiative Transfer **113**, 1683 (2012), ISSN 0022-4073, URL <http://www.sciencedirect.com/science/article/pii/S0022407312002336>.
 - ¹⁴ S.-i. Tamura, Phys. Rev. B **27**, 858866 (1983), URL <http://link.aps.org/doi/10.1103/PhysRevB.27.858>.
 - ¹⁵ F. H. Stillinger and T. A. Weber, Physical Review B **31**, 52625271 (1985).
 - ¹⁶ P. B. Allen and J. L. Feldman, Physical Review B **48**, 1258112588 (1993).
 - ¹⁷ R. Peierls, *Quantum Theory of Solids* (Oxford University Press, 2001).
 - ¹⁸ D. A. McQuarrie, *Statistical Mechanics* (University Science Books, Sausalito, 2000).
 - ¹⁹ Y. He, D. Donadio, and G. Galli, Applied Physics Letters **98**, 144101 (2011).
 - ²¹ D. G. Cahill and F. Watanabe, Phys. Rev. B **70**, 235322 (2004), URL <http://link.aps.org/doi/10.1103/PhysRevB.70.235322>.
 - ²² D. G. Cahill, F. Watanabe, A. Rockett, and C. B. Vining, Phys. Rev. B **71**, 235202 (2005), URL <http://link.aps.org/doi/10.1103/PhysRevB.71.235202>.
 - ²³ W. A. Kamitakahara and B. N. Brockhouse, Phys. Rev. B **10**, 12001212 (1974), URL <http://link.aps.org/doi/10.1103/PhysRevB.10.1200>.
 - ⁴⁴ A. Skye and P. K. Schelling, Journal of Applied Physics **103**, 113524 (2008), URL <http://link.aip.org/link/?JAP/103/113524/1>.
 - ⁴⁵ K. Momma and F. Izumi, Journal of Applied Crystallography **41**, 653658 (2008), URL <http://dx.doi.org/10.1107/S0021889808012016>.
 - ²⁶ J. V. Goicochea, M. Madrid, and C. H. Amon, Journal of Heat Transfer **132**, 012401 (2010).
 - ²⁸ D. P. Sellan, J. E. Turney, A. J. H. McGaughey, and C. H. Amon, Journal of Applied Physics **108**, 113524 (2010).
 - ²⁹ J. D. Gale and A. L. Rohl, Molecular Simulation **29**, 291 (2003).
 - ³⁰ J. C. Duda, T. S. English, D. A. Jordan, P. M. Norris, and W. A. Soffa, Journal of Physics: Condensed Matter **23**, 205401 (2011), URL <http://stacks.iop.org/0953-8984/23/i=20/a=205401>.
 - ³¹ A. M. Bouchard, R. Biswas, W. A. Kamitakahara, G. S. Grest, and C. M. Soukoulis, Phys. Rev. B **38**, 1049910506 (1988), URL <http://link.aps.org/doi/10.1103/PhysRevB.38.10499>.
 - ³² A. J. H. McGaughey and M. Kaviany, in *Advances in Heat Transfer, Volume 39*, edited by G. A. Greene, Y. I. Cho, J. P. Hartnett, and A. Bar-Cohen (Elsevier, 2006), p. 169255.
 - ³³ D. Donadio and G. Galli, Phys. Rev. Lett. **102**, 195901 (2009).
 - ³⁴ Y. He, D. Donadio, J.-H. Lee, J. C. Grossman, and G. Galli, ACS Nano **5**, 1839\961844 (2011).
 - ³⁵ P. B. Allen, J. L. Feldman, J. Fabian, and F. Wooten, Philosophical Magazine B **79**, 1715 (1999).
 - ³⁶ S. Volz and G. Chen, Physical Review B **61**, 26512656 (2000).
 - ³⁷ A. J. C. Ladd, B. Moran, and W. G. Hoover, Physical Review B **34**, 50585064 (1986).
 - ³⁸ J. E. Turney, PhD thesis, Carnegie Mellon University, Pittsburgh, PA (2009).
 - ⁴⁸ C. Kittel, Physical Review **75**, 974 (1949).
 - ⁴⁰ J. E. Graebner, B. Golding, and L. C. Allen, Phys. Rev. B **34**, 56965701 (1986), URL <http://link.aps.org/doi/10.1103/PhysRevB.34.5696>.
 - ⁴¹ D. J. Ecsedy and P. G. Klemens, Phys. Rev. B **15**, 59575962 (1977), URL <http://link.aps.org/doi/10.1103/PhysRevB.15.5957>.
 - ⁴² P. G. Klemens, Proceedings of the Physical Society. Section A **68** (1955).
 - ⁴³ P. G. Klemens, Proceedings of the Physical Society. Section A **70**, 833 (1957), URL <http://stacks.iop.org/0370-1298/70/i=11/a=407>.
 - ⁴⁷ S. Shenogin, A. Bodapati, P. Kebbinski, and A. J. H. McGaughey, Journal of Applied Physics **105**, 034906 (2009), URL <http://link.aip.org/link/?JAP/105/034906/1>.
 - ⁴⁶ V. Vitelli, N. Xu, M. Wyart, A. J. Liu, and S. R. Nagel, Phys. Rev. E **81**, 021301 (2010), URL <http://link.aps.org/doi/10.1103/PhysRevE.81.021301>.
 - ⁴⁹ P. Sheng and M. Zhou, Science **253**, 539542 (1991), URL <http://www.sciencemag.org/content/253/5019/539.abstract>.
 - ⁵⁰ N. Xu, V. Vitelli, M. Wyart, A. J. Liu, and S. R. Nagel, Phys. Rev. Lett. **102**, 038001 (2009), URL <http://link.aps.org/doi/10.1103/PhysRevLett.102.038001>.
 - ⁵³ K. Esfarjani and H. T. Stokes, Physical Review B **77**, 144112 (2008).
 - ⁵⁵ G. P. Srivastava, *The Physics of Phonons* (Adam Hilger, Bristol, 1990).
 - ⁵⁶ L. Landau, E. Lifshitz, and L. Pitaevskii, *Statistical Physics, Part 2 : Volume 9, Pt 2* (Elsevier Science & Technology Books, 1980), ISBN 9780750626361, URL <http://books.google.com/books?id=NaB7oAkon9MC>.

⁵⁸ J. A. Thomas, J. E. Turney, R. M. Iutzi, C. H. Amon, and A. J. H. McGaughey, Physical Review B **81**, 081411(R) (2010).

⁵⁹ Z.-Y. Ong, E. Pop, and J. Shiomi, Physical Review B **84**, 165418 (2011).

**

⁴⁹ For the disordered lattices studied in this work for $c \leq 0.15$, the predicted k_{AF} is strongly system size dependent, indicating this diverging behavior. For LJ argon alloys at $c = 0.5$, the divergence with system size is small for the range of system size studied ($N_0 = 4$ to $N_0 = 12$), where $k_{AF}/k_{GK} = 0.93$ for $N_0 = 12$. ††

⁵⁰ For a finite system, the AF theory requires a broadening

in frequency to predict the mode-specific thermal diffusivities. We use a Lorentzian broadening with a width of $\delta_{\omega,avg}$, see Section . ‡‡

⁵¹ Analysis of these high-frequency modes shows that they are locons, modes which are spatially localized in the Anderson sense. Feldman et al showed that the thermal diffusivities in a-Si show a sharp breakpoint at the onset of localized states, where it tends to zero exponentially. The correct length scale associated with these modes is the mode correlation length(cite), whose upper bound is the size of the simulation domain. §§

⁵² T